

Two-dimensional model simulation of Martian atmospheric convection with condensation of the major component under fixed thermal forcing

Tatsuya Yamashita*, Masatsugu Odaka*, Ko-ichiro Sugiyama**,[†], Kensuke Nakajima***, Masaki Ishiwatari*,[‡], Yoshiyuki O. Takahashi^{†,‡}, Seiya Nishizawa^{†,‡}, Yoshi-Yuki Hayashi^{†,‡}

* Department of CosmoSciences, Graduate School of Science, Hokkaido University

** Institute of Low Temperature Science, Hokkaido University

*** Department of Earth and Planetary Sciences, Faculty of Sciences, Kyushu University

[†] Department of Earth and Planetary Sciences, Graduate School of Science, Kobe University

[‡] Center for Planetary Science

1 Introduction

The observation by MOLA suggested that atmospheric major component, CO₂, condenses to form ice cloud in Martian polar region (Pettengill and Ford, 2000). The cloud echoes obtained by MOLA also suggested that some of the clouds are composed of large numbers of small particles. Colaprete *et al.* (2003) proposed that large numbers of small particles are not formed if there are no convective motion. However, based on conventional parcel theory, convection with condensation of the major component can not occur. The temperature profile of both an ascending air parcel and the surrounding environment follow the moist adiabat, and the air parcel can not gain buoyancy.

Colaprete *et al.* (2003) proposed that air parcel can gain buoyancy if supersaturation is sustained in the environment surrounding ascending air parcel. Laboratory experiments suggested that critical saturation ratio (the ratio of pressure to saturation vapor pressure at onset of condensation, hereafter written as S_{cr}) of 1.35 are required under the temperature and pressure in Martian polar region (Glandorf *et al.*, 2002). Colaprete *et al.* (2003) performed the numerical simulation for the case of $S_{cr} = 1.35$ and showed that strong vertical motion develops in the cloud. However, Colaprete *et al.* (2003) used a vertical one-dimensional model, and their purpose is to simulate an onset and initial expanding phase of a single cloud under a simplified and arbitrary initial condition.

With this background in mind, we have been developing a two-dimensional cloud resolving model (e.g.

Odaka *et al.*, 2006; Yamashita *et al.*, 2009, 2010). The purpose is to investigate a possibility that convection with condensation of the major component occur under the condition maintained by the statistical contribution of a large number of clouds over multiple cloud life cycles using long-term cloud resolving numerical simulations. In this work, we investigate dependence of convective structure on critical saturation ratio S_{cr} .

2 Model description

The used model are identical to those previously reported (Yamashita *et al.*, 2010). We review the model description briefly below.

We assume that the model atmosphere consists entirely of CO₂. The governing equations are based on the quasi-compressible equations (Klemp and Wilhelmson, 1978) and conservation equation of CO₂ vapor. The subgrid scale turbulence is implemented by the 1.5 order closure scheme (Klemp and Wilhelmson, 1978). The model atmosphere is subjected to an externally-given thermal forcing that is a substitute for the radiative cooling. The cloud microphysics is based on the parameterization scheme suggested by Tobie *et al.* (2003). In the scheme, only diffusion growth of CO₂ cloud particles is considered. We add a threshold of cloud density in order to inhibit unphysical condensation (Yamashita *et al.*, 2009); the threshold of cloud density is equivalent to considering the critical radius for nucleation implicitly. In the clear region, condensation occurs when saturation ratio exceeds critical saturation ratio S_{cr} . In the cloudy region, condensation occurs when saturation ratio exceeds 1.0, and cloud density

exceeds the threshold. For simplicity, in our calculation, we do not consider falling of cloud particle and drag force due to cloud particles.

We have chosen the spatially staggered mesh. Arakawa-C grid is employed for horizontal direction and Lorentz grid is employed for vertical direction. The space derivatives are approximated by the fourth-order centered difference scheme for advection terms and the second-order centered difference scheme for the other terms. In the grid point where negative cloud density is generated by using centered difference scheme, positive cloud density is transferred from surrounding points to the point so that the cloud density at the point is zero. Since the quasi-compressible system contains the acoustic mode in their solutions, the time step is severely restricted by the CFL condition for the phase speed of sound waves in the case a simple explicit time integration scheme is used. In order to save computational resources, the acoustic mode is integrated with a short time step and the other modes are integrated with a long time step (time-splitting method). The acoustic mode is treated by the HE-VI scheme. The horizontal propagation of sound waves is treated explicitly (Euler scheme) and the vertical propagation is treated implicitly (Crank-Nicolson scheme). The other modes are treated by the leap-frog scheme with Asselin time filter. Artificial viscosity terms are introduced for the sake of calculation stability.

The developed numerical models and documents are available in <http://www.gfd-dennou.org/library/deepconv/>.

3 Numerical configuration

The computational domain is 500 km in the horizontal direction and 25 km in the vertical direction. The spatial resolution is 200 m in both the horizontal and vertical directions. The short time step and the long time step are 0.125 sec and 1.0 sec, respectively. The cyclic boundary condition is applied in the horizontal direction. At the upper and lower boundary, the conditions of stress-free, no normal flow, no heat flux, and no CO₂ vapor flux are assumed. The initial temperature profile is given on the basis of a temperature profile in Martian winter polar cap (Colaprete and Toon, 2002). The temperature profile is dry adiabat below 4 km height, moist adiabat from 4 km to 15 km height, and isothermal (134 K) above 15 km height (Fig.1 left).

Random potential temperature perturbations ($\Delta\theta = 1$ K) are given at the lowest grid point to seed convective motion. We determine the initial pressure profile based on hydrostatic equation. We set the initial surface pressure to be 7 hPa.

We give horizontally uniform heating from 0 km to 1 km height, and horizontally uniform heating cooling from 1 km height to 15 km height. Cooling rate is set to be -5.0 K/day, and heating rate is adjusted so that the net heating is zero (Fig.1 right).

In our calculation, the values of critical saturation ratio $S_{cr} = 1.0$ and $S_{cr} = 1.35$ are used. Time integration is continued up to about 10 days (8.64×10^5 sec) in each case.

4 Results

We show the flow field at the time when the averaged atmospheric structure is well established and energy balance is nearly achieved in the case of both $S_{cr} = 1.0$ and 1.35.

4.1 The case for $S_{cr} = 1.0$

Above the condensation level (about 8 km height), horizontally uniform cloud layer are formed (Fig.2a). Below the condensation level, vertical temperature profile is almost dry adiabat. Hereafter, we call the region under the condensation level as “dry convective layer”.

Strong vertical motion occurs in the cloud layer, which is different from the prediction based on the conventional parcel theory. The distribution of mass stream function shows that a single-cell circulation whose vertical length scale is 20 km is formed (Fig.2b). Updraft in dry convective layer penetrates into the cloud layer, and downdraft in cloud layer penetrates into the dry convective layer. The maximum magnitude of the vertical velocity is about 20 m/sec (Fig.2c).

Contrary to the prediction based on the conventional parcel theory, the ascending parcels are subject to negative buoyancy in the cloud layer. Fig.2d shows the distributions of potential temperature deviation from the horizontally averaged profile. The buoyancy that an air parcel gain is proportional to the potential temperature deviation. The region where updraft exist ($x \sim 3.4 \times 10^5$ m) is warmer than their surrounding environment in the dry convective layer and colder in the cloud layer, and a schematic illustration of vertical distribution of poten-

tial temperature in the updraft is shown in Fig.3. The region where downdraft exist ($x \sim 0.9 \times 10^5$ m) is also warmer in the dry convective layer and colder in the cloud layer. This situation is uncommon in the Earth's atmosphere, because an air parcels gain buoyancy in the cloud in the case of Earth's moist convection. We discuss quantitatively how the ascending parcel gain buoyancy in section 5.

4.2 The case for $S_{cr} = 1.35$

As with the case of $S_{cr} = 1.0$, horizontally uniform cloud layer is formed above the condensation level (about 8 km height), and dry convective layer is formed below the condensation level (Fig.4a).

As with the case of $S_{cr} = 1.0$, strong vertical motion also occurs in the cloud layer. But in this case a number of convective cells are formed. The distribution of mass stream function shows that most of the convective cells have the vertical length scale of about 8 km and some of those have the scale of 20 km (Fig.4b). The distribution of vertical velocity shows that only strong updrafts in dry convective layer penetrate into cloud layer (Fig.4c). The maximum magnitude of upward velocity is about 15 m/sec which is small compared to the maximum magnitude of that in the case for $S_{cr} = 1.0$.

The distributions of potential temperature deviation from the horizontally averaged profile show that the magnitudes of the deviations near the condensation level are significantly large compared to other region (Fig.4d). Near condensation level, the regions where updrafts exist are colder than their surrounding environment and the regions where downdrafts exist are warmer than their surrounding environment. In the other region, The signs of the deviations are the same as those of $S_{cr} = 1.0$. The region where updrafts exist ($x \sim 3.4 \times 10^5$ m) are warmer than their surrounding environment in the dry region and colder in the cloud layer, and a schematic illustration of vertical distribution of potential temperature in the updraft is shown in Fig.5. These feature means that the ascending parcel is subject to negative buoyancy in cloud layer, especially near the cloud base. We also discuss quantitatively how the ascending parcel gain buoyancy in this case in section 5.

5 Discussions

The reason why strong updrafts occur in cloud layer in the case of both $S_{cr} = 1.0$ and 1.35 is that air parcels gain positive buoyancy sufficiently in dry convective layer. Fig.6 shows deviation of buoyancy from horizontal mean in the strongest updraft core (left) and the quantity which is obtained by integrating the deviation of buoyancy vertically from the surface (right) in the case of $S_{cr} = 1.0$. And Fig.7 is the same as in Fig.6 but for $S_{cr} = 1.35$. In the left panels of Fig.6 and 7, the signs of the deviations of buoyancy from horizontal mean are positive in the dry convective layer (below about 8 km), and negative in the cloud layer (above about 8 km), as mentioned in section 4. In the right panels of Fig.6 and 7, the sign is positive in the top (25 km), and this means that the net buoyancy is positive in both cases. That is, since the gain of buoyancy in dry convective layer is larger than the loss of buoyancy in cloud layer, the air parcel can penetrate into cloud layer. Gain of buoyancy in dry convective layer is not considered in the conventional parcel theory.

The difference of convective structure results from the loss of buoyancy near condensation level. Although ascending air parcel gain buoyancy in dry convective layer in the case of both $S_{cr} = 1.0$ and 1.35, the vertical motion in the case of $S_{cr} = 1.35$ is weaker than that in the case for $S_{cr} = 1.0$, as mentioned in section 4. It is because that loss of buoyancy in the case of $S_{cr} = 1.35$ is larger than that in the case of $S_{cr} = 1.0$ near condensation level. In the case of $S_{cr} = 1.35$, high supersaturation occurs in the ascending air parcel near the condensation level, and the parcel is subject to strong negative buoyancy force (Fig.5). Therefore some of the parcels can not penetrate into cloud layer, and circulations closed in dry convective layer are formed (Fig.4b). However, it should be noted that there is a possibility that the magnitude of negative buoyancy near the condensation level also depend on the large value of threshold of cloud density implemented in our model (it is equivalent to the case critical radius is about 10 μ m). If smaller value of threshold were to be implemented, the loss of buoyancy near condensation level will get smaller, and the flow field is expected to approach those in the case of $S_{cr} = 1.0$.

For future works, we are going to perform calculations with considering gravitational settling of cloud particles and drag force due to cloud particles. Numer-

ical experiments of cloud convection such as Nakajima *et al.*(1998) showed that gravitational settling and drag force of cloud particles affect the convective structure. Calculations with considering these effects are essential to investigate the structure of the convection which is established through a large number of life cycles of convective cloud elements.

Acknowledgement

Figures are plotted by using the softwares developed by Dennou Ruby Project (<http://ruby.gfd-dennou.org/>). Numerical calculations are performed by the NEC SX9 of the ISAS/PLAIN Center, JAXA.

References

- Colaprete, A., Toon, O. B., 2002: “Carbon dioxide snow storms during the polar night on Mars”, *J. Geophys. Res.*, **107**, 5051, doi:10.1029/2001JE001758.
- Colaprete, A., Haberle, R. M., Toon, O. B., 2003: “Formation of convective carbon dioxide clouds near the south pole of Mars. ” *J. Geophys. Res.*, **108**(E7), 5081, doi:10.1029/2003JE002053
- Glandorf, D. L., Colaprete, A., Tolbert, M. A., Toon, O. B., 2002: “CO₂ snow on Mars and early Earth: experimental constraints”, *Icarus*, **160**, 66 – 72.
- Klemp, J. B., Wilhelmson, R. B., 1978: “The simulation of three-dimensional convective storm dynamics”, *J. Atmos. Sci.*, **35**, 1070 – 1096.
- Nakajima, K., Takehiro, S., Ishiwatari, M., Hayashi, Y.-Y., 1998: “Cloud convections in geophysical and planetary fluids”(in Japanese), *Nagare Multimedia*, <http://www2.nagare.or.jp/mm/98/nakajima/index.htm>
- Odaka, M., Kitamori, T., Sugiyama, K., Nakajima, K., Takahashi, Y. O., Ishiwatari, M., Hayashi, Y.-Y., 2005: “A formulation of non-hydrostatic model for moist convection in the Martian atmosphere”, Proceeding of the 38 th ISAS Lunar and Planetary Symposium, 173 – 175.
- Odaka, M., Kitamori, T., Sugiyama, K., Nakajima, K., Hayashi, Y.-Y., 2006: “A numerical simulation of Martian atmospheric moist convection”(in Japanese), Proceeding of the 20 th ISAS Atmospheric Science Symposium, 103 – 106.
- Tobie, G., Forget, F., Lott, F., 2003: “Numerical simulation of winter polar wave clouds observed by Mars Global Surveyor Mars Orbiter Laser Altimeter”, *Icarus*, **35**, 33 – 49.
- Yamashita, T., Odaka, M., Sugiyama, K., Nakajima, K., Ishiwatari, M., Hayashi, Y.-Y., 2009: “A numerical simulation of Martian atmospheric moist convection”, Proceeding of the 42 th ISAS Lunar and Planetary Symposium, 12 – 16.
- Yamashita, T., Odaka, M., Sugiyama, K., Nakajima, K., Ishiwatari, M., Hayashi, Y.-Y., 2010: “Atmospheric convection with condensation of the major component”, Proceeding of the 43 th ISAS Lunar and Planetary Symposium, 7 pp.

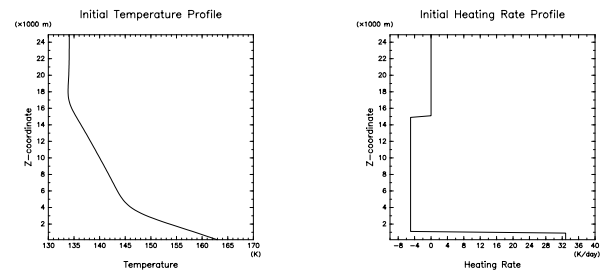
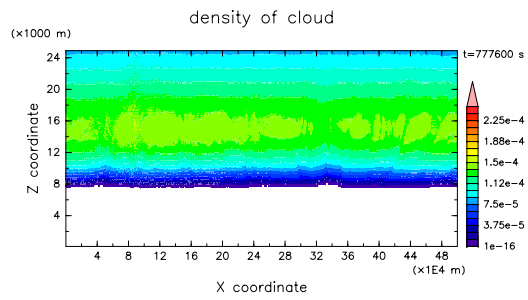
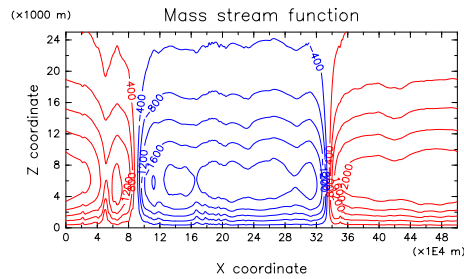


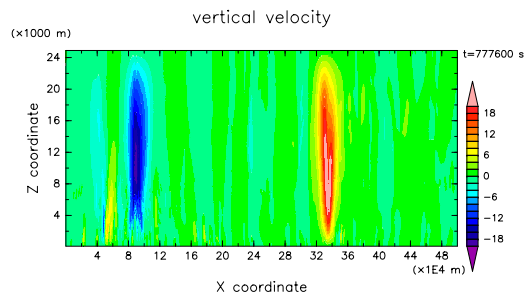
Figure 1: Initial temperature profile (left panel) and initial heating rate profile(right panel).



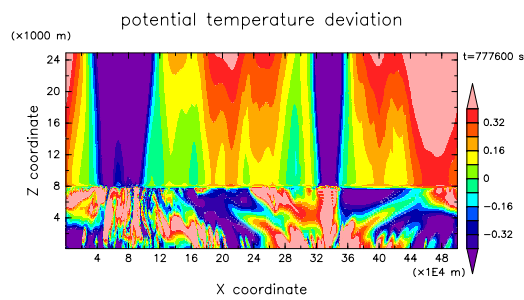
(a)



(b)



(c)



(d)

Figure 2: Snapshots for distribution of : (b) mass streamfunction, (a) density of cloud, (c) vertical velocity, and (d) deviation of potential temperature from horizontal mean at 7.776×10^5 sec in the case of $S_{cr} = 1.0$.

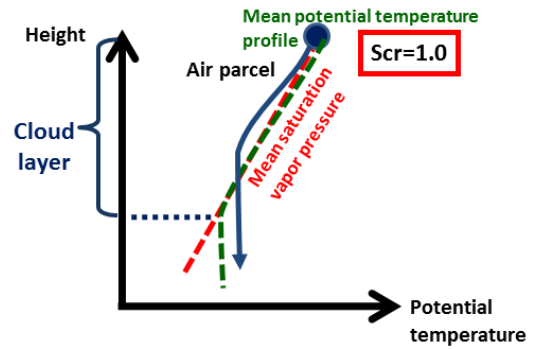
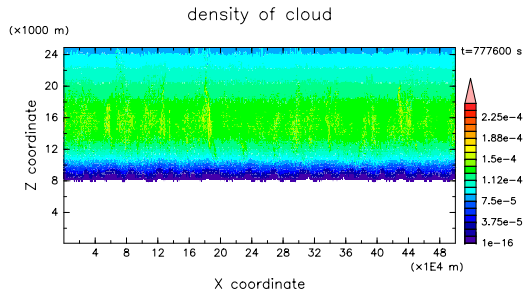
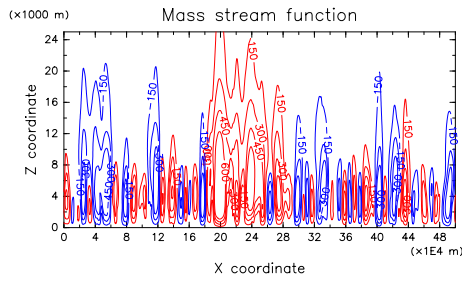


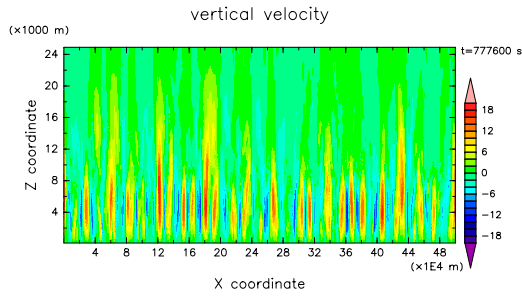
Figure 3: Schematic illustration of motion of an ascending air parcel in the case of $S_{cr} = 1.0$. The Red dashed line and the green dashed line indicate the potential temperature profile which has moist adiabatic lapse rate, and mean potential temperature profile, respectively.



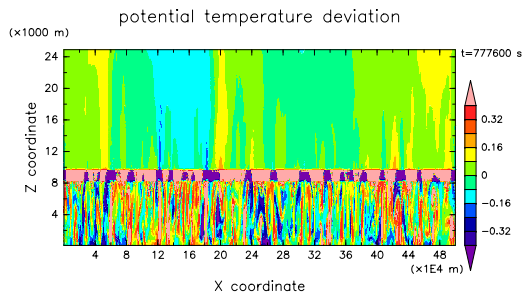
(a)



(b)



(c)



(d)

Figure 4: Same as in Fig. 2b, 2a, 2c and 2d but for $S_{cr} = 1.35$.

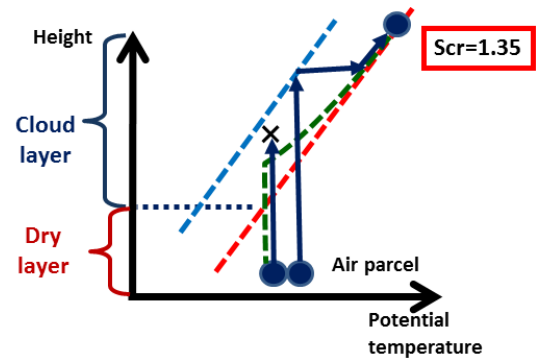


Figure 5: Same as in Fig.3 but for $S_{cr} = 1.35$. The blue dashed line indicates the potential temperature profile in which saturation ratio is 1.35.

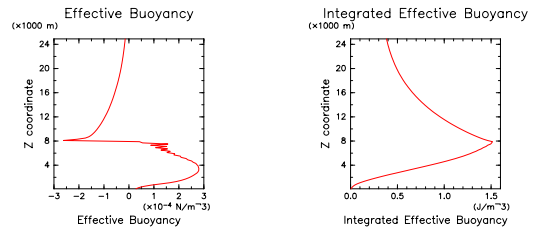


Figure 6: The deviation of buoyancy from horizontal mean in updraft core ($x \sim 3.4 \times 10^5$ m) in the case of $S_{cr} = 1.0$ (left panel) and the quantity which is obtained by integrating the deviation of buoyancy vertically from the surface (right panel).

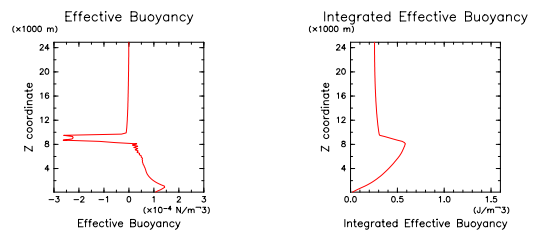


Figure 7: The deviation of buoyancy from horizontal mean in updraft core ($x \sim 0.9 \times 10^5$ m) in the case of $S_{cr} = 1.35$ (left panel) and the quantity which is obtained by integrating the deviation of buoyancy vertically from the surface (right panel).